Isolation of crystals of a planar nitronyl nitroxide radical: 2-phenylbenzimidazol-1-yl *N*,*N*′-dioxide (PBIDO)

Yoshio Kusaba,[a,b] Masafumi Tamura,*[a]† Yuko Hosokoshi,[a]‡ Minoru Kinoshita,[a]§ Hiroshi Sawa,[a]¶ Reizo Kato[a] and Hayao Kobayashi[b]‡

[a]*The Institute for Solid State Physics, Roppongi, Minato-ku, Tokyo 106, Japan*
[b]*Department of Chemistry, Faculty of Science, Toho University, Miyama 2-2-1, Funabashi, Chiba 274, Japan*

A planar nitronyl nitroxide radical, 2-phenylbenzimidazol-1-yl *N*,*N*′-dioxide, has been isolated in a stable single crystal form. X-Ray analysis has shown that the radical molecules form a dimeric two-dimensional structure. The dominant magnetic interactions have been found to be antiferromagnetic. Anomalous temperature dependence of susceptibility was observed below 10 K. The EPR study indicates that this is ascribable to spin-multiplet states generated in the crystal.

The study of stable organic radicals has been extended more and more, particularly in accordance with the recent progress in molecular magnetism.[1] For the control of magnetic interactions and magnetism in the solid state, numerous strategies have been proposed on the basis of various factors operating in radical crystals.[1]

The neutral radical crystals studied so far are composed of molecules with non-planar and flexible substituents, such as methyl and *tert*-butyl groups. One of the roles of such substituents is structural hindrance to decomposition;[2] they are believed to stabilize the radicals chemically. On the other hand, the existence of such flexible units on the molecule sometimes gives rise to an unexpected structural phase transition at low temperature due to the structural degrees of freedom.[3]

The appreciably high stability of the phenyl nitronyl nitroxide radicals,[4] which can be explained in terms both of the conjugation over the two NO groups and of large negative charges on the terminal oxygen atoms, brings the idea that the nitronyl nitroxide moiety may still retain its stability even if the usual tetramethylethylene burdening is replaced by an aromatic ring. This idea does not sound so hopeless, because the resultant structure still contains no hydrogen on the α-carbon atom. The expected structural stiffness of such a molecule may reduce the structural instability and may lead to a well-organized crystal structure; only the rotation around the C—C bond linking the phenyl and benzimidazole groups remains flexible. Moreover, the imidazole ring fused with another aromatic ring is expected to provide a new way to control the spin density distribution over each molecule in the solid state. This extension of molecular design would afford new features in intra- and inter-molecular magnetic interactions and may contribute to a new design of stable radical species of interest.

We have succeeded in isolating such a radical, 2-phenylbenzimidazol-1-yl *N*,*N*′-dioxide (**1**, abbreviated as PBIDO)[5–8] in crystalline form. This molecule consists only of planar units. This is the first example of the above extension of the repertory of isolable organic radicals. The crystals were so stable that we were able to study them by X-ray crystallography and make magnetic measurements, although this compound was put into the unisolable category in ref. 2. We report here the preparation, X-ray structure and magnetism of the crystals of this radical.

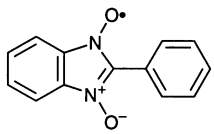

PBIDO **1**

Experimental

X-Ray crystallography

X-Ray intensity data at 298 K were collected for a single crystal with dimensions $0.10 \times 0.10 \times 0.05$ mm, using a MAC Science automated four-circle diffractometer MXC18 with graphite monochromatized Cu-Kα radiation by θ–2θ scans up to $2\theta = 130°$. 1528 independent reflection data satisfying $|F| > 3\sigma(|F|)$ were used for the structural analysis. The structure was solved by the direct method and refined by full-matrix least-squares analysis with an anisotropic approximation except hydrogen atoms. An analytical absorption correction was made. All the procedures were carried out with the CRYSTAN program package by MAC Science.‖

Powder X-ray diffraction data were collected using a MAC Science MXP18 System with a rotating anode generator and a monochromator of single crystalline graphite for Cu-Kα radiation.

Static magnetic susceptibility measurements

Magnetic susceptibilities were measured for a polycrystalline sample from 300 to 1.8 K, by use of a Quantum Design MPMS SQUID magnetometer. Below 10 K, the applied field was kept as low as 400 Oe in order to avoid saturation effects. The data were corrected for diamagnetic contributions, by subtracting the diamagnetic contribution estimated from the curve-fitting described below.

Present Addresses
† Department of Physics, Faculty of Science, Toho University, Miyama 2-2-1, Funabashi, Chiba 274, Japan (tamura@ph.sci.toho-u.ac.jp).
‡ Institute for Molecular Science, Myodaiji, Okazaki, Aichi 444, Japan.
§ Science University of Tokyo in Yamaguchi, Daigaku-dori 1-1-1, Onoda, Yamaguchi 756, Japan.
¶ Department of Physics, Faculty of Science, Chiba University, Yayoicho 1-33, Inage-ku, Chiba 263, Japan.

‖ Atomic coordinates, thermal parameters, and bond lengths and angles have been deposited at the Cambridge Crystallographic Data Centre (CCDC). See Information for Authors, *J. Mater. Chem.*, 1997, Issue 1. Any request to the CCDC for this material should quote the full literature citation and the reference number 1145/34.

EPR measurements

EPR spectra were recorded using a JEOL JES FE1XG X-band spectrometer. The samples were placed at the centre of a cylindrical cavity operating in the TE011 mode. For the low temperature measurements, a helium-flow type cryostat (Air Products LTR-3-110) was used to cool the sample to 2.3 K.

Results and Discussion

Preparation of the radical crystal

The target radical was generated by oxidation of 1-hydroxy-2-phenylbenzimidazole N^3-oxide, **2** (Scheme 1). For the synthesis of **2**, various methods have been reported.[9–14] Schemes 2 and 3 show the two pathways to the precursor **2** applied in this work. All the reactions in Schemes 2 and 3 were carried out by following literature procedures.[9,14–18] The only modification was that we used sulfuric acid instead of perchloric acid[18] in the coupling reaction of benzaldehyde, **3**, and *o*-benzoquinone dioxime, **9**. Scheme 3 was simpler, in spite of the relatively low yield of the *o*-benzoquinone dioxime. Nitrosobenzene, **7**, and benzofuroxan, **8**, were commercially obtained.

The oxidation of **2** was carried out using excess PbO_2 in CH_2Cl_2 or by aqueous $NaIO_4$. However, the latter gave a sizable amount of by-product, reducing the yield of **1**. Therefore, we obtained **1** for the crystallization and physical measurements mainly by use of PbO_2. Prior to the oxidation, **2** was purified by dissolution in a 14% aqueous solution of NaOH and reprecipitation by addition of 6 mol dm^{-3} HCl to it. To a suspension of 0.50 g of **2** in 100 ml of CH_2Cl_2, typically 30 g of powdered PbO_2 was added and stirred for 10 min to yield a slightly yellowish light-green solution of **1**. The residual mixture was filtered off and was put into another 100 ml of CH_2Cl_2 followed by stirring for 10 min. The reaction in CH_2Cl_2 and filtering were repeated three times, until the filtrate became almost colourless. All the filtrate was again filtered and evaporated to dryness under reduced pressure. The yield was 0.39 g (78%). Overnight reaction with PbO_2 resulted in decomposition of **1**.

Single crystals of **1** were obtained by evaporation of a pentane solution of **1** (30 mg in 100 ml) for *ca.* 2 h. Rhombic plate-like dark-brown crystals were collected after washing with hexane. Other solvents, such as ethanol, diethyl ether, acetone and benzene, gave rise to partial decomposition of the radical during evaporation, as noted by white precipitation or colour change of solution from light green to brown. Calc. for $C_{13}H_9N_2O_2$: C, 69.33; H, 4.03; N, 12.44%. Found: C, 69.04; H, 4.09; N, 12.46%.

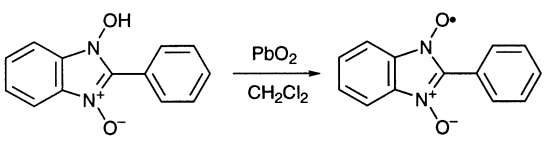

2 **1**

Scheme 1

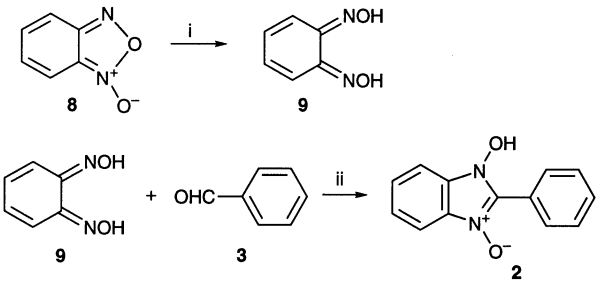

8 **9** **9** **3** **2**

Scheme 3 *Reagents and conditions*: i, $NH_2OH \cdot HCl$–MeOH, 25% KOH–H_2O, 30 min (ref. 18); ii, H_2SO_4–EtOH, reflux overnight (ref. 14)

EPR spectra of CH_2Cl_2 solutions of the obtained crystals of **1** recorded under air showed clear 1:2:3:2:1 five-split lines due to the two equivalent ^{14}N nuclei in the molecule. The observed coupling constant, $\alpha_N = 4.2$ Oe, was consistent with those reported previously.[5–8]

Powder X-ray diffraction was also examined for the powdered solid of **1**. A total of 25 diffraction peaks were observed between $5 < 2\theta < 40^\circ$. All these peaks can be indexed in terms of the lattice parameters of the crystal structure described below.

Crystal structure

The molecular structure of the radical **1** is displayed in Fig. 1. The benzimidazole skeleton including the terminal oxygen atoms is almost planar, as well as the phenyl ring. The dihedral angle between the best planes for the benzo and ONCNO moieties is 1.06°. Moreover, the dihedral angle between the best planes for the ONCNO moiety and the phenyl ring is only 10.29°; the molecule is nearly coplanar overall.

Our idea that the stability of nitronyl nitroxides requires little stereochemical hindrance, as mentioned in the Introduction, has thus been demonstrated. In solution, the stability of the radical **1** is somewhat reduced when compared to that of the conventional nitronyl nitroxides with the burden of the saturated ethylene. However, the isolated crystals of **1** were stable enough to examine the structure and magnetic properties without any special care. This is a rare example of a neutral organic radical having a nearly planar structure in a purely crystalline form.

The crystallographic data are summarized in Table 1. The crystal belongs to the orthorhombic system with the space group *Pcab*. The lattice constants are, $a = 11.483(1)$, $b = 23.655(2)$, $c = 7.7924(6)$ Å, $V = 2116.6$ Å^3 and $Z = 8$. The final positional parameters are listed in Table 2. The molecular arrangement is what is called the κ-structure[19] in the field of molecular conductors, *i.e.* two-dimensional packing of dimers, spreading over the *ac*-plane (Fig. 2). All the dimers are crystallographically equivalent and centrosymmetric. They are formed by ring-over-ring overlap of benzimidazole units [Fig. 3(*a*)].

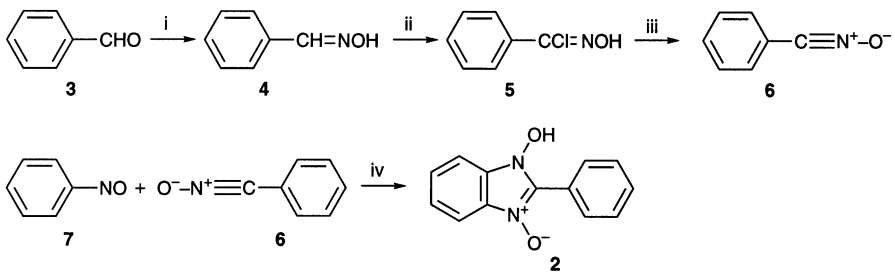

3 **4** **5** **6** **7** **6** **2**

Scheme 2 *Reagents and conditions*: i, $NH_2OH \cdot HCl$–EtOH, conc. NaOH, 2 h, then dry ice (ref. 15); ii, Cl_2, 8 M HCl (ref. 16); iii, 14% NaOH, 15 min (ref. 17); iv, Et_2O, 30 min (ref. 9)

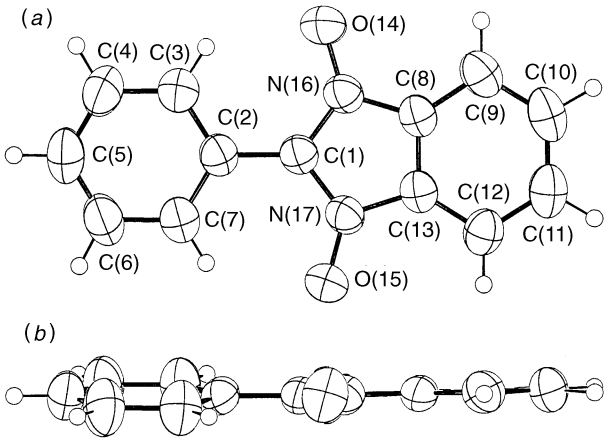

Fig. 1 Molecular structure of PBIDO in the crystal. (*a*) Viewed along the direction normal to the imidazole plane. Atomic numbering scheme is also shown. (*b*) Viewed along the O···O direction.

Table 1 Crystallographic data of PBIDO

formula	$C_{13}H_9N_2O_2$
formula mass	225.20
crystal size/mm	$0.10 \times 0.10 \times 0.05$
crystal system	orthorhombic
space group	*Pcab*
V/Å^3	2116.6(4)
a/Å	11.483(1)
b/Å	23.655(2)
c/Å	7.7924(6)
Z	8
D_c/g cm^{-3}	1.41
radiation	Cu-Kα ($\lambda = 1.54178$ Å)
scan mode	θ–2θ
total reflections measured	2151
unique reflections	1778
reflections used ($\|F_o\| > 3\sigma(\|F_o\|)$)	1528
residuals: R; R_w[a]	0.048; 0.057
goodness of fit: S	1.63

[a]The function minimized was sum $[w(|F_o|^2 - |F_c|^2)^2]$, in which $w = 1/[\sigma(|F_o|)^2]$.

Table 2 Positional parameters and equivalent isotropic thermal parameters with standard deviations in parentheses

atom	x	y	z	B(eq)
C (1)	0.1120 (2)	−0.10374 (8)	0.3752 (2)	4.0 (1)
C (2)	0.1209 (2)	−0.16429 (8)	0.4038 (2)	4.3 (1)
C (3)	0.2177 (2)	−0.1875 (1)	0.4851 (3)	6.1 (1)
C (4)	0.2251 (2)	−0.2450 (1)	0.5126 (4)	7.0 (1)
C (5)	0.1373 (2)	−0.2805 (1)	0.4603 (3)	6.4 (1)
C (6)	0.0424 (2)	−0.2583 (1)	0.3790 (4)	6.9 (1)
C (7)	0.0333 (2)	−0.2007 (1)	0.3511 (3)	5.9 (1)
C (8)	0.1447 (2)	−0.00892 (8)	0.3874 (2)	4.2 (1)
C (9)	0.1880 (2)	0.04410 (9)	0.4230 (3)	5.2 (1)
C (10)	0.1281 (2)	0.0887 (1)	0.3477 (3)	6.0 (1)
C (11)	0.0318 (2)	0.0802 (1)	0.2439 (3)	5.7 (1)
C (12)	−0.0107 (2)	0.02659 (9)	0.2092 (3)	5.0 (1)
C (13)	0.0494 (2)	−0.01736 (8)	0.2841 (2)	4.1 (1)
O (14)	0.2692 (1)	−0.06990 (7)	0.5425 (2)	6.0 (1)
O (15)	−0.0518 (1)	−0.09843 (6)	0.1896 (2)	6.0 (1)
N (16)	0.1824 (1)	−0.06285 (6)	0.4420 (2)	4.3 (1)
N (17)	0.0303 (1)	−0.07633 (7)	0.2770 (2)	4.2 (1)
H (3)	0.277 (2)	−0.162 (1)	0.517 (4)	6.12 (0)
H (4)	0.293 (3)	−0.260 (1)	0.568 (4)	6.97 (0)
H (5)	0.144 (2)	−0.320 (1)	0.481 (4)	6.36 (0)
H (6)	−0.022 (2)	−0.282 (1)	0.342 (4)	6.86 (0)
H (7)	−0.033 (2)	−0.185 (1)	0.301 (4)	5.93 (0)
H (9)	0.256 (2)	0.050 (1)	0.492 (4)	5.23 (0)
H (10)	0.159 (2)	0.126 (1)	0.361 (4)	5.95 (0)
H (11)	−0.010 (2)	0.112 (1)	0.192 (3)	5.73 (0)
H (12)	−0.077 (2)	0.020 (1)	0.139 (3)	4.97 (0)

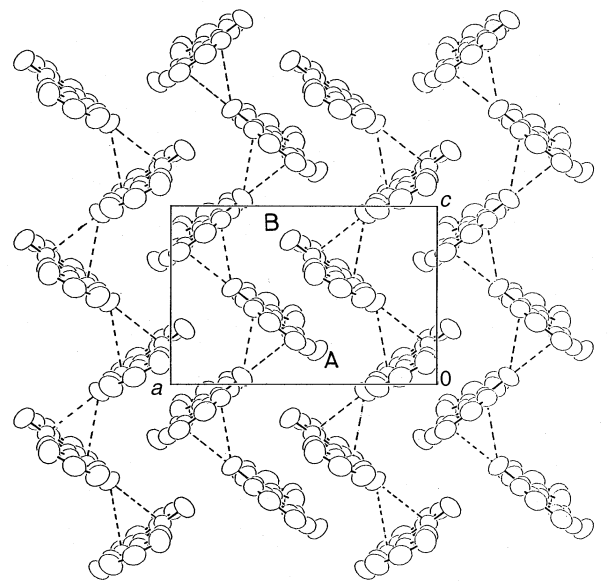

Fig. 2 Molecular packing viewed along the *b*-axis. Broken lines show the short distances; O(14)···N(17) 2.943 and O(14)···N(16) 3.166 Å.

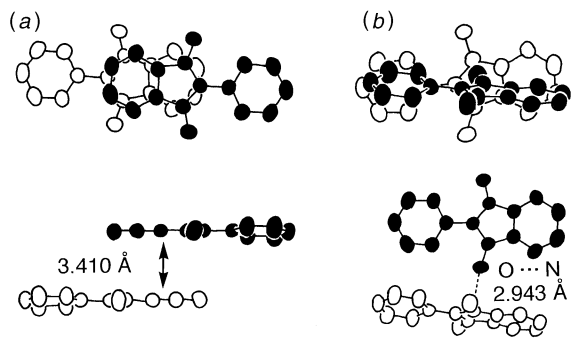

Fig. 3 (*a*) Face-to-face overlapping within the dimer. (*b*) The interdimer close spacing.

The distance between the best planes of benzimidazole units within the dimer is 3.410 Å. This face-to-face packing should provide sizable antiferromagnetic intradimer coupling due to overlap integral between the SOMOs. The molecules are nearly orthogonal between the adjacent dimers [Fig. 3(*b*)]. Relatively short intermolecular interatomic distances are found between the terminal oxygen atom and the imidazole unit. For example, the interatomic distances around 3 Å are O(14)···N(17) 2.943, O(14)···C(1) 3.037, O(14)···N(16) 3.166 and O(14)···C(8) 3.206 Å. As shown by de Panthou *et al.*[20] and by Inoue and Iwamura,[21] this kind of contact has possibilities of ferromagnetic coupling due to the orthogonality between the SOMOs. However, the conditions for this are rather subtle and it would be easily masked by the larger antiferromagnetic intradimer contributions.

Static magnetic susceptibility

The temperature dependence of the paramagnetic susceptibility (χ_p) measured for a polycrystalline sample of **1** is depicted in Fig. 4. It exhibited a rounded maximum at *ca.* 45 K. Below this temperature, χ_p steeply decreased to *ca.* 10 K. With more cooling, χ_p again increased down to 3 K, where another small maximum appeared. The χ_p value at the second maximum amounts to approximately a third of that at the first maximum, and is close to that at room temperature. As shown in the inset of Fig. 4, χ_p gradually decreased to 1.8 K, indicating that the χ_p value extrapolated to $T = 0$ is finite. Such behaviour

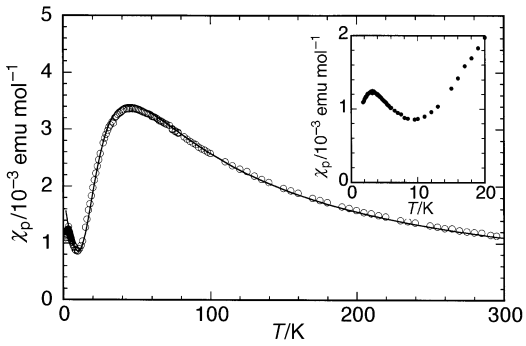

Fig. 4 Temperature dependence of the paramagnetic susceptibility. Solid curve shows the fit to eqn. (3). The inset shows a close-up of the low temperature region.

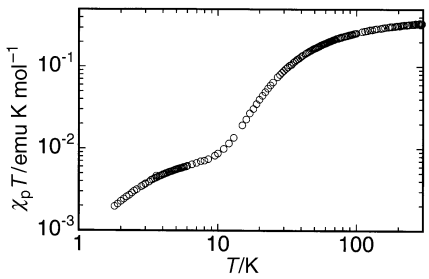

Fig. 5 Log–log plot of $\chi_p T$ *vs.* T

(finite χ_p towards $T=0$) qualitatively resembles that of a gapless low-dimensional antiferromagnetic system, *e.g.* a spin-1/2 uniform chain.[22]

This low-temperature behaviour of χ_p, the appearance of a second maximum and the slow decrease below 3 K, seems peculiar and puzzling, although it was reproducible. We suspected that this might be due to some lattice imperfection introduced with cooling. Therefore, we examined the dependence of the behaviour on cooling rate; we compared the susceptibility data for a slowly cooled (12 h from 290 to 4 K) sample and those for a rapidly cooled (several minutes from 290 to 4 K) one. However, both were the same. It is not easy to attribute the peculiar magnetic behaviour to the effect of lattice imperfections.

The appearance of the first larger χ_p maximum indicates that the dominant intermolecular interactions are antiferromagnetic. It is most likely that the distinct dimeric structure having face-to-face overlap gives rise to such a large antiferromagnetic coupling. If the intradimer coupling only is relevant, the system reduces to a simple singlet–triplet model, eqn. (1),

$$H = 2J_1 \sum_j \boldsymbol{S}_j \cdot \boldsymbol{S}_j' \quad (1)$$

where J_1 (<0) denotes the intradimer exchange coupling, and S_j and S_j' stand for the spin-1/2 operators for the molecules within the j th dimer. The model shows the paramagnetic susceptibility as given by eqn. (2),

$$\chi_{p,dimer} = (C/T)3/[3 + e^{-2J_1/k_B T}] \quad (2)$$

with $C = 0.50$ emu K mol^{-1} for $g=2$. This gives a broad maximum at $T = -1.247 J_1/k_B$ where $\chi_{p,dimer} = 0.151/(J_1/k_B)$ emu mol^{-1}. Qualitative agreement of the observed χ_p with this model is found. However, a satisfactory fit over a wide temperature range could not be obtained by this model; the $\chi_{p,dimer}$ value at the peak exceeds the observed χ_p value. Therefore, interactions other than intradimer ones should be considered to account for the temperature dependence of χ_p.

A better fit was obtained when we used the formula for χ_p in eqn. (3),

$$\chi_p = \chi_{p,dimer}/[1 - 2\langle zJ_2\rangle \chi_{p,dimer}/N_A g^2 \mu_B^2] + C'/(T-\theta') \quad (3)$$

where the first term corresponds to the major contribution showing the larger maximum and the second term represents the tail of the low temperature component. The first term is the first-order correction of $\chi_{p,dimer}$ for the mean-field $\langle zJ_2\rangle$ stemming from the interdimer interactions, J_2, where z is the number of nearest-neighbour dimers and the other symbols have their usual meanings. We obtained $C = 0.48$ emu K mol^{-1}, $J_1/k_B = -38$ K, $\langle zJ_2\rangle/k_B = -17$ K, $C' = 1.3 \times 10^{-2}$ emu K mol^{-1} and $\theta' = 6.5$ K. However, this is not entirely justified because $\langle zJ_2\rangle$ is comparable to J_1; it is not appropriate to regard $\langle zJ_2\rangle$ as a simple mean field in such a case. Moreover, the mean field becomes meaningless at lower temperatures because the number of triplet species decreases with temperature. Therefore, this analysis does not give more than a qualitative estimate. We can conclude that $J_1/k_B \approx -40$ K and the interdimer interactions are antiferromagnetic whose order of magnitude is $J_2/k_B \sim -10$ K.

For the sake of estimating the contribution of the low temperature component of χ_p, which is responsible for the appearance of the second maximum, the product $\chi_p T$ is plotted against temperature in Fig. 5. Since $\chi_p T$ is proportional to the square of the so-called effective moment, this plot often gives insight into magnetic interactions in a crystal. The high temperature $\chi_p T$ value is consistent with the paramagnetic spin-1/2 behaviour, which yields $\chi_p T \rightarrow 0.375$ emu K mol^{-1} with $g=2$ to the limit $T \rightarrow \infty$. The monotonic decrease in $\chi_p T$ with cooling to low temperature again indicates that sizeable antiferromagnetic coupling is operating. At *ca.* 10 K, where the peculiar behaviour was observed, the $\chi_p T$ value is *ca.* 7×10^{-3} emu K mol^{-1}, *ca.* a fiftieth of the high temperature value. In other words, the number of spins responsible for the peculiar behaviour is less than a fiftieth of the total number. This is consistent with the above analysis of χ_p, where $C'/C \approx 1/50$ was obtained. It is almost not possible to derive a physical model explaining such a fact from the highly symmetric and simple molecular packing at room temperature. At present, we can only point out that one possible origin may be the effect of crystal surface or edge, long-range lattice modulation, or systematically introduced dislocations.

Solid state EPR spectra

Single crystals of **1** exhibit an exchange-narrowed single EPR line at room temperature. The principal g-values for the static field ($\boldsymbol{H}$) applied along the three crystal axes are, $g_a = 2.0083$, $g_b = 2.0059$ and $g_c = 2.0057$. This is consistent with the orientation of the ONCNO moieties in the crystal; it is known that most spin density is concentrated on the ONCNO moiety in the nitronyl nitroxides. Therefore, no drastic change of this character occurs in our case. The largest peak-to-peak linewidth, $\Delta H_{pp} = 3.8$ Oe, was observed when $\boldsymbol{H} \| \boldsymbol{b}$, the normal direction to the *ac*-plane. With tilting the field toward the in-plane directions, *a* or *c*, the line became narrower, showing a minimum near magic angle (Fig. 6). Such behaviour is characteristic of a two-dimensional spin arrangement.

In order to probe the low temperature magnetism micro-

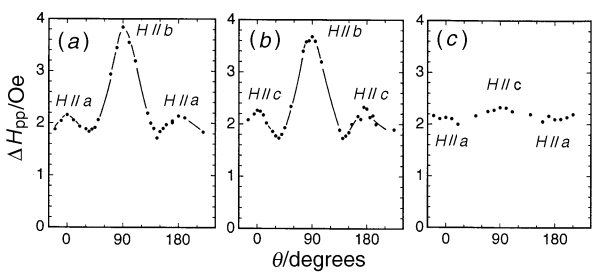

Fig. 6 Angle dependence of the EPR linewidth at 290 K

scopically, the temperature dependence of the results was EPR investigated. Fig. 7 shows the temperature dependence of spin susceptibility (χ_{spin}) obtained from the EPR spectra. The susceptibilities are basically isotropic and show temperature dependence similar to that by static measurements. The temperature dependence of the *g*-value was very weak for each field directions.

Below *ca.* 10 K, the EPR line broadens, and fine structure satellites appear below *ca.* 4 K as shown in Fig. 8. The splitting width of the fine structure is largest in the $\boldsymbol{H}\|\boldsymbol{a}$ spectrum; it amounts to *ca.* 60 Oe. The width was smallest when the field is tilted from the *a*-direction by *ca.* 60°, indicating that the dipolar interaction responsible for the fine structure links the spins placed along the *a*-axis. In addition to this, $\Delta m_s = 2$ transition near $H = 1600$ Oe became observable below 4 K (Fig. 9). These features indicate that spin-multiplet states are formed in the crystal at low temperature. It is also found that the additional enhancement of susceptibility below 10 K comes from the growing contributions of the fine structure. The decrease in χ_p and χ_{spin} below 3 K indicates that some weak antiferromagnetic coupling is operating over the multiplet states. The largest splitting width of the fine structure for the $\boldsymbol{H}\|\boldsymbol{a}$ spectrum is a measure of twice zero-field splitting parameter, *i.e.* 2*D ca.* 60 Oe. In terms of the point–dipole approximation, this corresponds to the dipolar coupling between two spin-1/2 species spaced by *ca.* 10 Å. This is close to the lattice period $a = 11.483$ Å: the distance between the second-nearest-neighbouring dimers. It is therefore likely that the multiplet state is formed over the dimers along the *a*-axis, although its origin and detailed mechanism are still in question. More detailed analyses, as well as other physical measurements, are now underway.

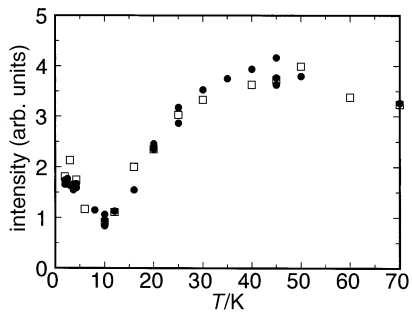

Fig. 7 Temperature dependence of the EPR intensity (spin susceptibility) for (●) $\boldsymbol{H}\|\boldsymbol{a}$, (□) $\boldsymbol{H}\|\boldsymbol{b}$

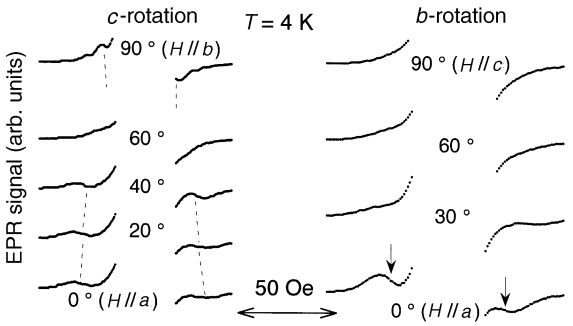

Fig. 8 Low temperature EPR spectra showing fine structure. The strong central lines are omitted for clarity.

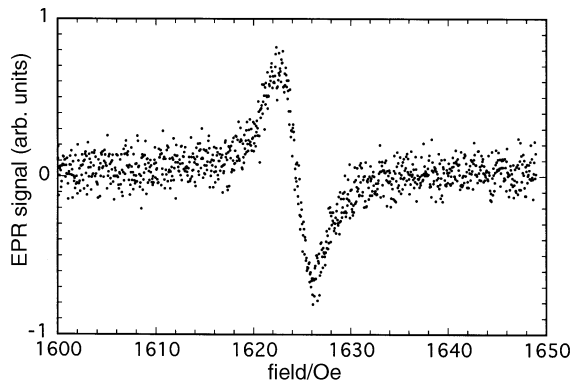

Fig. 9 The $\Delta m_s = 2$ resonance observed at 4 K

Conclusion

It has been demonstrated that the planar organic radical PBIDO can be isolated as a sufficiently stable single crystal, although its stability in solution is somewhat lower than those of conventional nitronyl nitroxides. The successful crystallization of this planar radical would expand the possible range of design directed to molecular magnetism. The PBIDO molecules are arranged in a dimeric fashion and form a layered structure in the crystal. The dominant magnetic interactions are intradimer antiferromagnetic, *i.e.* J_1/k_B *ca.* −30 K, while the weaker antiferromagnetic interactions, J_2/k_B *ca.* −10 K, are operative between the dimers. Peculiar behaviour of χ_p, the second small maximum, was observed below 10 K. Only 1/50 spins are responsible for this anomaly. The EPR studies have revealed that this is related to the appearance of spin-multiplet states at low temperature. The physical mechanism behind the low temperature behaviour is in question. Any model applied to this should explain the following features: (*i*) the 1/50 spin number, (*ii*) appearance of the EPR fine structure and (*iii*) gapless susceptibility behaviour at very low temperature.

We are indebted to Dr Akihiko Hayashi and Professor Yutaka Ueda for their help with the powder X-ray measurements. We would like to thank Dr Daisuke Shiomi and Mr Kiyokazu Nozawa for valuable discussions and experimental support. This work is partly supported by the Grant-in-Aid for Scientific Research on Priority Area 'Molecular Magnetism' (Area No. 228/04242103) from the Ministry of Education, Science and Culture, Japan. Financial supports from the New Energy and Industrial Technology Development Organization (NEDO) and Toyota Physical and Chemical Research Institute are also acknowledged.

References

1 For example, see: D. Gatteschi, *Adv. Mater.*, 1994, **6**, 635; M. Kinoshita, *Jpn. J. Appl. Phys.*, 1994, **33**, 5718; J. S. Miller and A. J. Epstein, *Angew. Chem., Int. Ed. Engl.*, 1994, **33**, 385. See also, *Proc. 4th Int. Conf. Molecule-Based Magnets, Salt Lake City*, 1994, ed. J. S. Miller and A. J. Epstein, *Mol. Cryst. Liq. Cryst.*, 1995, 271–274; K. Togashi, R. Imachi, K. Tomioka, H. Tsuboi, T. Ishida, T. Nogami, N. Takeda and M. Ishikawa, *Bull. Chem. Soc. Jpn.*, 1996, **69**, 2821, and references cited therein.
2 J. F. W. Keana, *Chem. Rev.*, 1978, **78**, 37, and references cited therein.
3 D. Shiomi, M. Tamura, H. Aruga Katori, T. Goto, A. Hayashi, Y. Ueda, H. Sawa, R. Kato and M. Kinoshita, *J. Mater. Chem.*, 1994, **4**, 1915; Y. Hosokoshi, M. Tamura, M. Kinoshita, H. Sawa, R. Kato, Y. Fujiwara and Y. Ueda, *J. Mater. Chem.*, 1994, **4**, 1219.
4 E. F. Ullman, J. H. Osiecki, D. G. B. Boocock and R. Darcy, *J. Am. Chem. Soc.*, 1972, **94**, 7049.
5 A. T. Balaban, P. J. Halls and A. R. Katritzky, *Chem. Ind.*, 1968, 651.
6 H. G. Aurich and W. Weiss, *Chem. Ber.*, 1973, **106**, 2408.
7 H. G. Aurich and K. Stork, *Chem. Ber.*, 1975, **108**, 2764.
8 T. E. Gough and R. Puzic, *J. Magn. Reson.*, 1976, **23**, 31.
9 F. Minisci, R. Galli and A. Quilico, *Tetrahedron Lett.*, 1963, 785.
10 A. J. Boulton, A. C. G. Gray and A. R. Katritzky, *J. Chem. Soc. (B)*, 1968, 911.

11 D. W. S. Latham, O. Meth-Cohn and H. Suschitzky, *J. Chem. Soc., Chem. Commun*., 1972, 1040.
12 D. W. S. Latham, O. Meth-Cohn, H. Suschitzky and J. A. L. Herbert, *J. Chem. Soc., Perkin Trans. 1*, 1977, 470.
13 H. N. Borah, R. C. Boruah and J. S. Sandhu, *Heterocycles*, 1985, **23**, 1625.
14 F. Pätzold, H.-J. Niclas and E. Gründemann, *J. Prakt. Chem*., 1990, **332**, 345.
15 J. S. Buck and W. S. Ide, *Org. Synth*., 1943, **Coll. Vol. II**, 622.
16 O. Piloty and H. Steinbeck, *Berichte*, 1902, **35**, 3112.
17 G. W. Perold, A. P. Steyn and F. V. K. von Reiche, *J. Am. Chem. Soc*., 1957, **79**, 462.
18 T. Zincke and P. Schwarz, *Annalen*, 1899, **307**, 28.
19 For example, see: R. Kato, H. Kobayashi, A. Kobayashi, S. Moriyama, Y. Nishio, K. Kajita and W. Sasaki, *Chem. Lett*., 1987, 507; H. Urayama, H. Yamochi, S. Sato, A. Kawamoto, J. Tanaka, T. Mori, Y. Maruyama and H. Inokuchi, *Chem. Lett*., 1988, 463; D. Jung, M. Evain, J. J. Novoa, M.-H. Whangbo, M. A. Beno, A. M. Kini, A. J. Schultz, J. M. Williams and P. J. Nigrey, *Inorg. Chem*., 1989, **28**, 4516.
20 F. L. de Panthou, D. Luneau, L. Laugier and P. Rey, *J. Am. Chem. Soc*., 1993, **115**, 9095.
21 K. Inoue and H. Iwamura, *Chem. Phys. Lett*., 1993, **207**, 551.
22 J. C. Bonner and M. E. Fisher, *Phys. Rev*., 1964, **135**, A640.

Paper 6/08399D; *Received* 16*th December*, 1996